Journal of Power Sources 258 (2014) 290–296

Contents lists available at ScienceDirect

Journal of Power Sources

journal homepage: www.elsevier.com/locate/jpowsour

Synthesis of porous graphene/activated carbon composite with high packing density and large specific surface area for supercapacitor electrode material

Chao Zheng, Xufeng Zhou*, Hailiang Cao, Guohua Wang, Zhaoping Liu*

Ningbo Institute of Materials Technology and Engineering, Chinese Academy of Sciences, Zhejiang 315201, PR China

HIGHLIGHTS

- Porous graphene/activated carbon was prepared via hydrothermal carbonization and subsequent two-step chemical activation.
- The composites owe a high packing density and has a specific capacitance of 210 F g^{-1}.
- A high capacity retention rate of 94.7% after 5000 cycles can be achieved.

ARTICLE INFO

Article history:
Received 18 August 2013
Received in revised form
3 January 2014
Accepted 14 January 2014
Available online 14 February 2014

Keywords:
Graphene
Activated carbon
Hydrothermal carbonization
Chemical activation
Supercapacitor

ABSTRACT

A simple method has been developed to prepare graphene/activated carbon (AC) nanosheet composite as high-performance electrode material for supercapacitor. Glucose solution containing dispersed graphite oxide (GO) sheets is hydrothermally carbonized to form a brown char-like intermediate product, and finally converts to porous nanosheet composite by two-step chemical activation using KOH. In this composite, a layer of porous AC coats on graphene to from wrinkled nanosheet structure, with length of several micrometers and thickness of tens of nanometer. The composite has a relatively high packing density of ~0.3 g cm^{-3} and large specific surface area of 2106 m^2 g^{-1}, as well as containing plenty of mesopores. It exhibits specific capacitance up to 210 F g^{-1} in aqueous electrolyte and 103 F g^{-1} in organic electrolyte, respectively, and the specific capacitance decreases by only 5.3% after 5000 cycles. These results indicate that the porous graphene/AC nanosheet composite prepared by hydrothermal carbonization and chemical activation can be applied for high performance supercapacitors.

1. Introduction

Supercapacitor – also called electrochemical capacitor – is a new electrochemical energy storage system applied for harvesting energy and delivering high power in short time. Its main energy storage mechanism is based on charging an electrical double-layer (EDL) at the electrode–electrolyte interface of high surface area electrode materials. They have attracted attention for a variety of applications, especially in hybrid systems combining with batteries and fuel cells, due to their high power density, excellent cyclic stability and rapid response to external loading on a powertrain [1–4]. Nevertheless, the main disadvantage of supercapacitor is the relatively low energy density (5–6 Wh kg^{-1} based on activated carbon, AC), which is significantly lower than that of lithium ion rechargeable battery (~150 Wh kg^{-1}). Therefore, the most important issue for supercapacitor research is to enhance its energy density. Many efforts have been focused on developing new kinds of electrode materials, such as carbon nanotubes (CNTs) [5,6], graphene [7,8] and CNTs/graphene hybrid materials [9,10], as well as transition metal oxides [11,12] and conductive polymers [13–15] having pseudocapacitive behaviors. Unfortunately, up to now only AC has been commercially used as supercapacitor electrode materials due to its well-developed microstructure, high specific surface area, relatively high packing density, and low cost. However, their applications account for only a comparatively small market because of its low energy density. On the other hand, the AC particles usually have sizes up to several tens of micrometers, which results in a long diffusion pathway for ions, as well as relatively low conductivity. These disadvantages make AC unfavorable in the process of rapid charge/discharge and for the requirement of excellent cyclability. For the AC materials, to enhance surface area as well as

* Corresponding authors. Tel./fax: +86 574 86685096.
E-mail addresses: zhouxf@nimte.ac.cn (X. Zhou), liuzp@nimte.ac.cn (Z. Liu).

http://dx.doi.org/10.1016/j.jpowsour.2014.01.056
0378-7753/

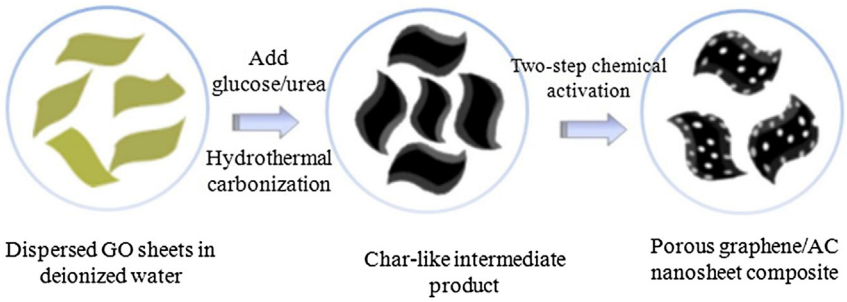

Fig. 1. Schematic illustration showing the experimental steps of preparing porous graphene/AC nanosheet composite.

maintain high packing density, control pore size distribution, reduce diffusion resistance and improve conductivity are still challenging.

Graphene [16], a two-dimensional carbon material consisting of a single-layer of sp^2 hybridized carbon atoms, has been considered as an outstanding candidate electrode material for supercapacitors due to its unique properties, such as exceptionally high specific surface area (2630 $m^2\ g^{-1}$, higher than that of CNTs and commercial AC, and major surface of graphene is exterior surface readily accessible by electrolyte), excellent electrical conductivity and stable chemical properties. Most significantly, the intrinsic capacitance of graphene was found to be 21 μF cm^{-2} [17]. Thus, the theoretical value of graphene is calculated to be 550 F g^{-1}, provided the entire surface is fully utilized. Many works have been reported based on graphene and modified graphene [18–20] for supercapacitors. Unfortunately, the EDL capacitance value measured is far lower than the theoretical one, mainly because that graphene sheets have inevitable tendency to restack themselves during all procedures of graphene preparation and subsequent electrode production. Meanwhile, the low packing density with a value as low as 0.005 g cm^{-3} is another drawback of graphene. In the past, many works were interested in the materials with high specific surface area, and the specific capacitance per unit weight is mostly adopted to judge the performance of the electrode materials. However, the specific capacitance per unit volume (Wh L^{-1}) is of prime importance for practical applications as the space for the

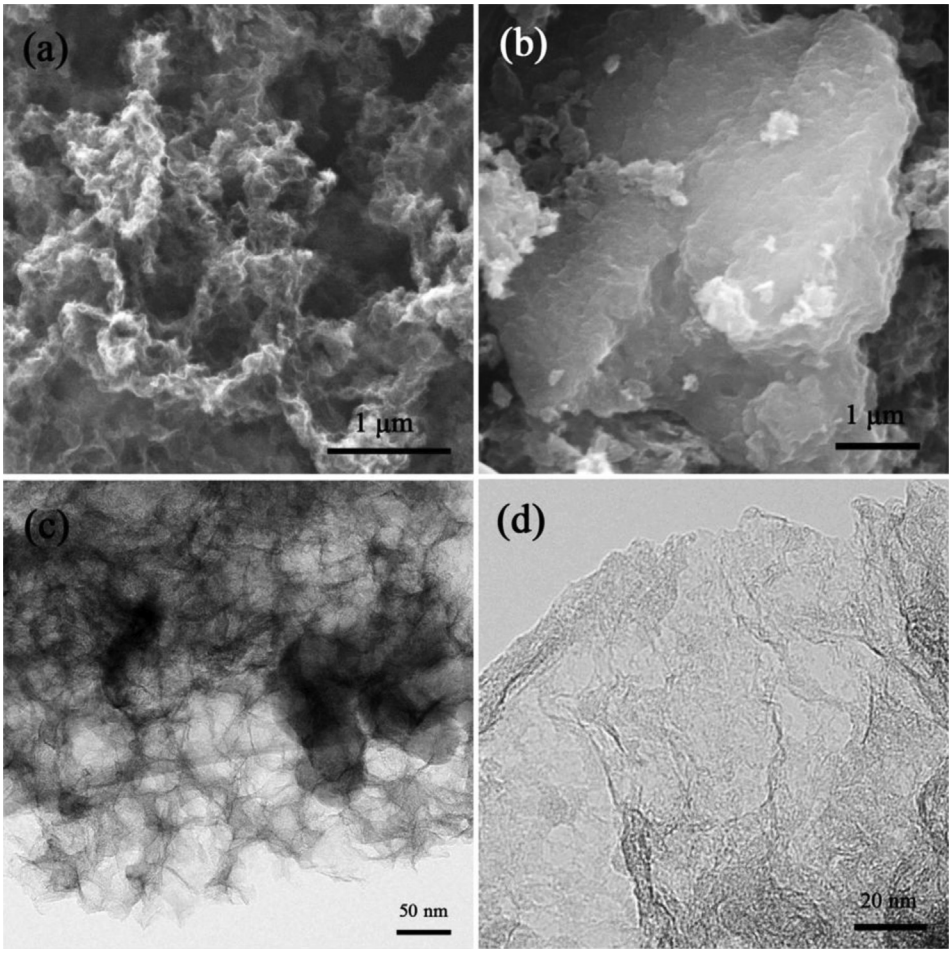

Fig. 2. (a) SEM image of char-like intermediate product, (b) SEM image of graphene/AC nanosheet composite, (c), (d) TEM images of graphene/AC nanosheet composite.

power unit is always limited. The volumetric capacitance is mainly affected by the packing density of electrode materials. However, it is usually difficult to achieve high volumetric density and high surface area simultaneously for graphene due to its unique sheet-like morphology. Therefore, how to enhance the packing density of graphene while still maintaining high surface area is highly desirable and imperative.

Hybrid carbon materials as electrode materials, for example graphene/CNTs composite, have been reported to enhance the electrochemical performance. Generally, the combination of different carbon materials with different structural features and physicochemical properties will give rise to better performance comparing with that of single component due to the synergistic effect [9,21]. Inspired by the above, we have prepared porous graphene/AC nanosheet composite via hydrothermal carbonization and subsequent two-step chemical activation with KOH. In the composite, a layer of porous AC is coated on graphene sheets, which not only inhibits agglomeration and increases surface area, but also enhances packing density. On the other hand, integrating graphene into AC matrix will notably increase conductivity of AC. Comparing to large AC particles, it is worth pointing out that the nanosheet composite will reduce the diffusion pathway significantly. Results from measurement of electrochemical performance suggest that the obtained graphene/AC nanosheet composite exhibits high capacitance and excellent cycling stability. The relatively high packing density and good electrochemical performance as well as the low-cost preparation process make graphene/AC nanosheet composites potentially applicable for high-performance supercapacitors.

2. Experimental

2.1. Sample preparation

Graphene oxide (GO) powder used in this work was obtained by chemical exfoliation of natural graphite following the modified method as described elsewhere. The experimental steps shown in Fig. 1 is similar to that described in our previous work [22]. Briefly, 0.15 g of obtained GO powder was firstly added into 120 ml of deionized water and then dispersed by ultrasonication with power of 300 W for 30 min. After that, 6.0 g of urea and 4.5 g of glucose were added. After ultrasonication for another 30 min, the mixture was transferred into a 150 ml Teflon autoclave and hydrothermally treated at 180 °C for 24 h. After filtering and washing with deionized water for three times, the obtained solid sample was dried at 80 °C under vacuum for 10 h. 0.81 g of intermediate product was obtained.

The chemical activation was carried out in two steps. Firstly, the intermediate product was mixed with KOH with a weight ratio of 1:4 and was chemically activated at 850 °C for 2 h in Ar atmosphere. The obtained sample was washed with 15 wt.% HCl solution and then washed to neutral with deionized water, and then dried at 120 °C for 12 h. Secondly, the same KOH treatment procedure described above was applied for re-activation. As a result, 0.25 g of graphene/AC composite was obtained.

2.2. Structural characterizations

The as prepared samples were characterized by a Hitachi S-4800 field emission scanning-electron microscopy (SEM) and a FEI Tecnai G^2 F20 transmission electron microscopy (TEM). The nitrogen sorption isotherm (BET) was recorded by a Micromeritics ASAP-2020 M nitrogen adsorption apparatus. Pore size distribution plot was obtained by the Barrett–Joyner–Halenda (BJH) method. Powder X-ray diffraction (XRD) measurements were analyzed by an AXS D8 Advance diffractometer (Cu Kα radiation; receiving slit, 0.2 mm; scintillation counter, 40 mA; 40 kV) from Bruker Inc. Raman spectroscopy plots were obtained by a Renishaw inVia Reflex confocal microscopy Raman spectrometer (laser wavenumber 532 nm).

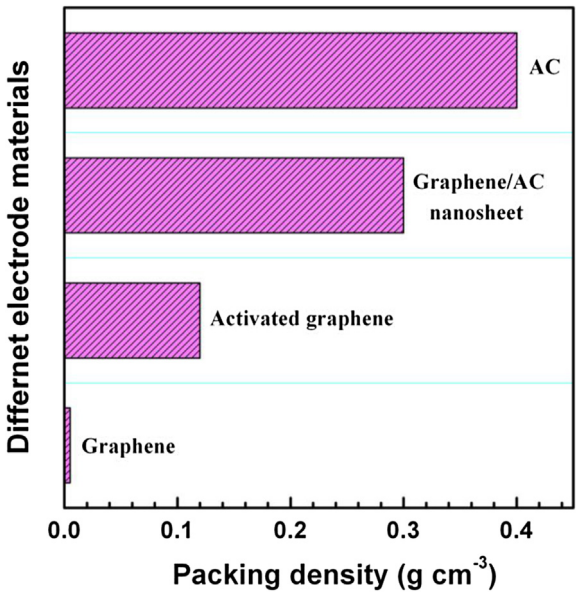

Fig. 3. Packing density comparison of different electrode materials.

2.3. Electrochemical tests

The evaluation of electrochemical performance was carried out in CR2032 coin cells. Both 6 M KOH aqueous solution and 1 M Et_4NBF_4/PC were used as the electrolytes. For the coin cells tested in aqueous solution, the working electrode contained 90 wt. % of active material and 10 wt. % of poly(terafluoroethylene) (PTFE). For comparison, coin cells using commercial AC (YP-50F, Kuraray Co.,

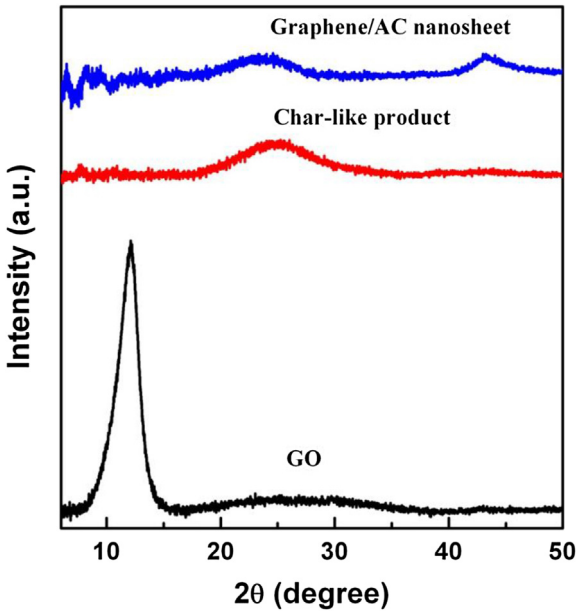

Fig. 4. XRD patterns of the pristine GO, char-like intermediate product and the as-prepared graphene/AC nanosheet composite.

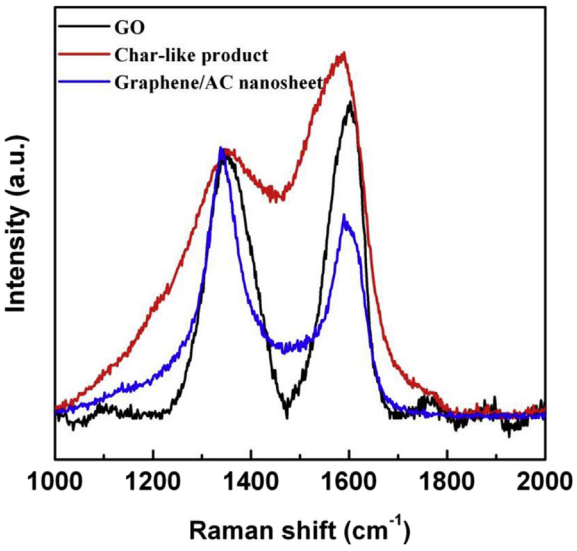

Fig. 5. Raman spectra of the pristine GO, char-like intermediate product and the as-prepared graphene/AC nanosheet composite at the wavelength of 532 nm.

Ltd. packing density ~0.4 g cm^{-3}, specific surface area ~1600 m^2 g^{-1}) as the active material was also made with an electrode composition of 80 wt.% AC powder, 10 wt.% PTFE and 10 wt.% carbon black. The electrochemical performance such as cyclic voltammetry (CV) and electrochemical impedance spectroscopy (EIS) were characterized by using a Solartron Instrument Mode 1470E electrochemical workstation at ambient condition. For the test in organic electrolyte, 10 wt. % of polyvinylidene fluoride (PVDF) was used as the binder. The CV curve and specific capacitance were measured under different scan rates of 0–200 mV s^{-1} between 0 and 2.5 V, and the cycling ability was tested under 100 mV s^{-1} for 5000 cycles.

3. Results and discussion

Pristine GO powder was firstly dispersed as nearly single-layered sheets in glucose solution by ultrasonication. Then, a brown char-like intermediate product was achieved by hydrothermal carbonization, whose morphology was shown in Fig. 2a. It's clearly seen that the intermediate product still has the thin-sheet like structure similar to that of graphene, though severe aggregation occurs. The relatively larger sheet thickness as well as wrinkled and rough surface suggests that a layer of amorphous carbon was uniformly coated on the hydrothermally reduced GO sheets. After the subsequent procedure of two-step chemical activation by the use of KOH at high temperature, the color of the sample became black. In the high magnification SEM image, the sample exhibits wrinkled nanosheet morphology, with thickness of tens of nanometers (Fig. 2b). The TEM images (Fig. 2c and d) further clearly indicate that the KOH activation process can effectively etch the intermediate product to form porous nanosheet composite. The packing density of graphene/AC was measured and compared with other carbon materials as shown in Fig. 3. Graphene/AC composite has a value of ~0.3 g cm^{-3}, which is far more than that of graphene (0.005 g cm^{-3}) and activated graphene (0.12 g cm^{-3}), close to that of commercial AC (~0.4 g cm^{-3}). Such improvement can be ascribed to the hybrid structure, in which a layer of porous AC was coated on graphene to form thicker sheets than pure graphene. The relatively high packing density of graphene/AC composite is beneficial for practical applications.

Fig. 4 shows the XRD patterns of the pristine GO, char-like intermediate product and the graphene/AC nanosheet composite. GO shows a sharp diffraction peak at $2\theta = 12.1°$, and no obvious peak at the position of the (002) peak of graphite (about 26°) is observed, indicating that the graphite has been fully expanded. The *d*-spacing value is 0.73 nm, which suggests the presence of oxygen-functional groups for the basal plane of the graphene layers in graphite [23]. After hydrothermal carbonization with urea for 24 h, the intermediate product exhibits a weak and broad diffraction peak at $2\theta = 25.0°$ and the sharp diffraction peak of GO disappeared. The *d*-spacing value significantly decreased to 0.35 nm, suggesting that most oxygen-functional groups intercalated into the interlayer spacing of graphite were removed during the hydrothermal carbonization process. Urea has been reported as a reducing agent for effective reduction of GO. The presence of urea can promote the removal of oxygen-functional groups and restore π-conjugation structure, due to the volatile reducing gases produced during hydrothermal carbonization [24]. Finally, the (002) peak of graphene/AC nanosheet composite further weakens and broadens, probably because the particle size of the composite was reduced during the chemical activation process.

Fig. 5 shows the Raman spectra of the pristine GO, char-like intermediate product and the graphene/AC nanosheet composite. The Raman spectrum of GO displays a D-band at ~1351 cm^{-1} and G-band at ~1602 cm^{-1}. The G-band originates from the in-phase vibration of the graphite lattice, while the D-band mainly comes

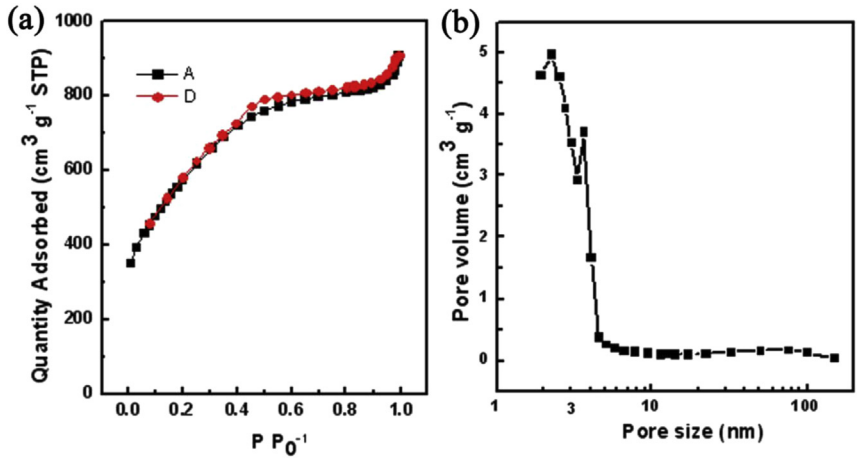

Fig. 6. (a) Nitrogen adsorption/desorption isotherms and (b) pore size distribution curve of the graphene/AC nanosheet composite.

from the structure defects created by the attachment of oxygen-functional groups on the carbon basal plane. The intensity ratio of D-band to G-band (I_D/I_G value) is 0.84, indicating the high oxidation degree and/or relatively small domain size. After hydrothermal carbonization, the D-band and G-band broaden significantly and display a shift to lower frequencies, which maybe ascribe to the presence of amorphous carbon produced during hydrothermal carbonization. The I_D/I_G ratio was decreased to 0.74, which indicates considerable recovery of the conjugated graphite network by removing the oxygen-functional groups during this process. In addition, the I_D/I_G ratio was significantly increased to 1.32 after KOH chemical activation, which is contributed to the creation of defects of the sample. In this case, the increased defect degree is apparently due to the increased ratio of sp^3 hybridized carbon near the edges of the pores etched by KOH, as shown in Fig. 2d.

The nitrogen adsorption/desorption isotherms of the graphene/AC nanosheet composite at 77 K and the corresponding pore size distribution are shown in Fig. 6. The isotherms of composite sample can be identified as type IV according to the IUPAC classification. A hysteresis loop could be observed in the range of 0.4–0.8 P P_0^{-1}, suggesting the presence of mesopores, which was further identified in the pore size distribution profile (Fig. 6b) calculated from the desorption branch using the BJH model. The mean pore size is 2–4 nm. Unlike one-step chemical activation (the dominant pore is micropore) [25], two-step chemical activation is an effective way to convert part of micropores to mesopores. These mesopores can facilitate the rapid transport and migration of electrolyte ions during the charge/discharge process, which is suitable for high-rate supercapacitor with high power density. In addition, the composite exhibits a BET surface area of 2106 $m^2\ g^{-1}$, which is close to the theoretical value of graphene and far more than that of thermally reduced graphene. According to the EDLC energy storage mechanism, the huge surface area will allow graphene/AC electrode with high energy density.

CV is mostly used as a suitable tool to characterize the capacitive behavior and to quantify the specific capacitance of an electrode material. Fig. 7a shows the CV curves of graphene/AC nanosheet composite at different scan rates ranging from 1 to 200 mV s^{-1} within a potential range of 0–1 V in 6 M KOH solution. It is obvious that all of the CV curves exhibit nearly ideal rectangular shape, indicating that the specific capacitance primarily originates from the double-layer capacitance based on ions adsorption/desorption. Since the oxygen-functional groups were mostly removed during the high temperature thermal treatment, the contribution of pseudocapacitance is negligible. The shapes of CV curves do not change remarkably as the scan rate is increased from 1 to 200 mV s^{-1}, reflecting fast charge transfer within the composite material, which is resulted from the two-dimensional nanosheet morphology of the sample along with suitable pore size. The specific capacitance as a function of the scan rate for graphene/AC composite and commercial AC is compared in Fig. 7b. All capacitance results were obtained by CV measurements under different scan rates in the ranges of 0–200 mV s^{-1}. The specific capacitance of graphene/AC composite is up to 210 F g^{-1} at 1 mV s^{-1}, which is far higher than that of the commercial AC (76 F g^{-1} at 1 mV s^{-1}). For both electrodes, further increasing the scan rate results in the decrease of the specific capacitance of the electrode, due to the mass transfer limitation of ions inside electrode material at high current densities. However, at any scan rate, the graphene/AC composite electrodes exhibited higher capacitance compared to commercial AC electrode. The specific capacitance for graphene/AC composite is still higher than 100 F g^{-1} at a high scan rate of 200 mV s^{-1}.

The EIS analysis is one of principal methods to examine the fundamental behavior of electrode materials for supercapacitor.

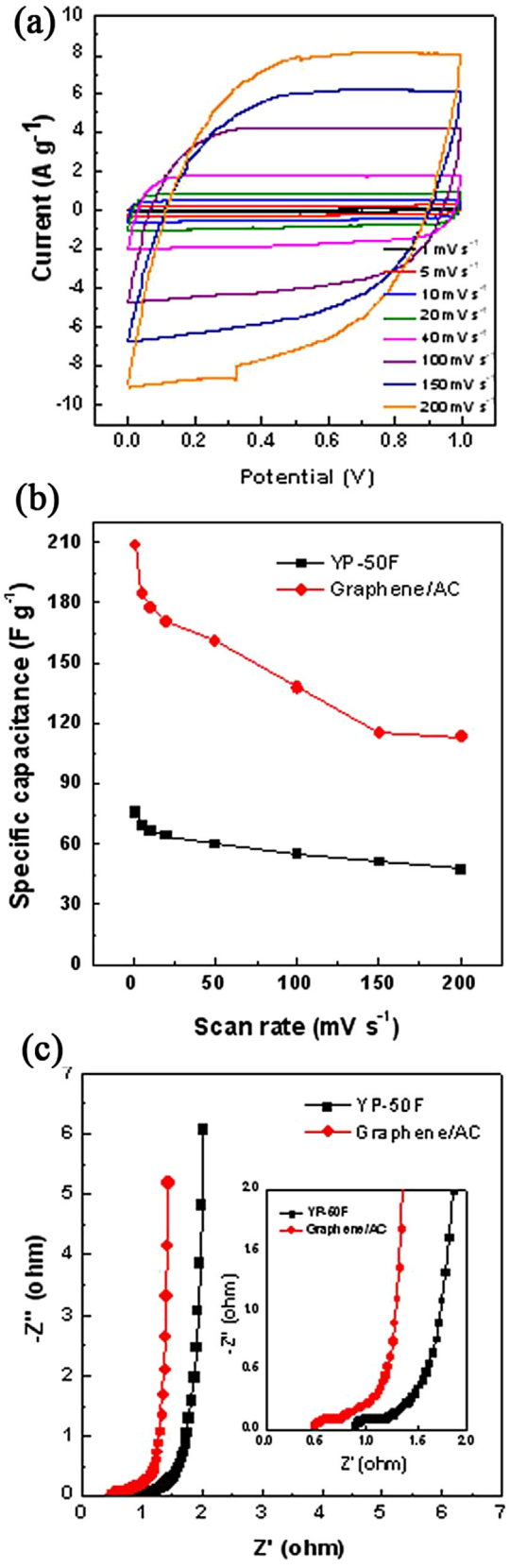

Fig. 7. (a) CV curves of graphene/AC nanosheet composite electrode at different scan rates within a potential range of 0–1 V in 6 M KOH aqueous electrolyte, (b) the specific capacitance of graphene/AC nanosheet composite electrode and commercial AC electrode at different scan rates, and (c) the Nyquist plots of graphene/AC nanosheet composite electrode and commercial AC electrode (the inset shows the enlarged EIS at high frequency region).

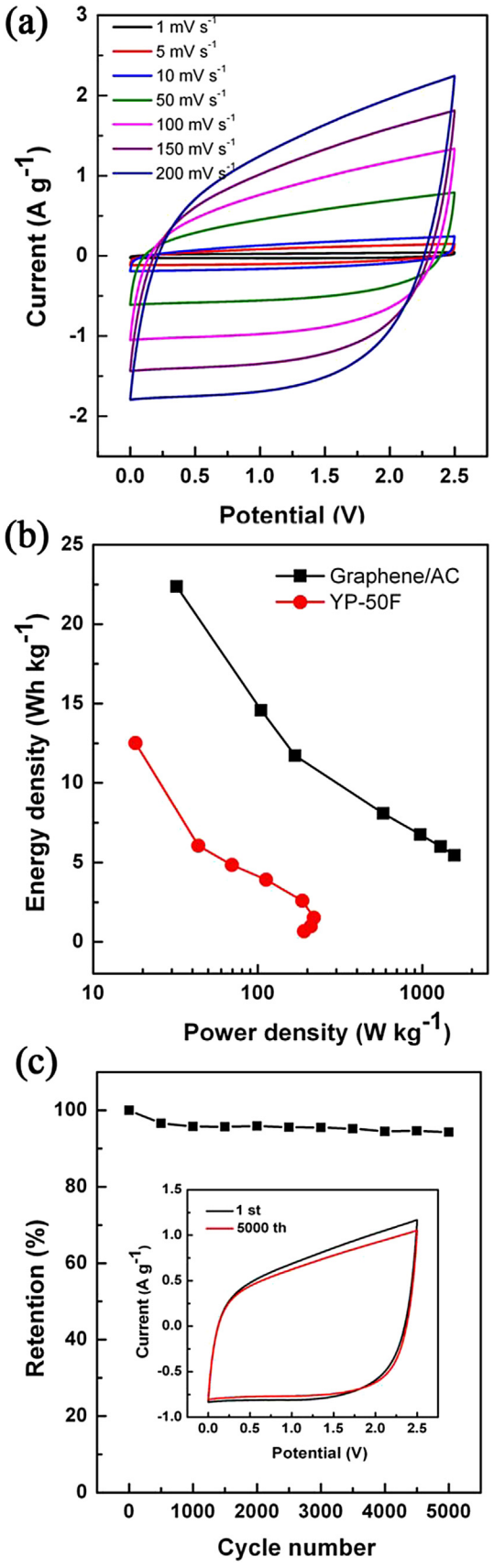

Fig. 8. (a) CV curves of graphene/AC nanosheet composite electrode at different scan rates within a potential range of 0–2.5 V in 1 M Et_4NBF_4/PC solution, (b) the Ragone plots of graphene/AC composite electrode and commercial AC electrode, and (c) long-term cycling performance of the graphene/AC nanosheet composite electrode measured at 100 mV s^{-1}.

The Nyquist plots for graphene/AC composite electrode and commercial AC electrode are shown in Fig. 7c. Both Nyquist plots are similar in form, consisting of one small semicircle at high frequency and an apparent straight line in the low frequency region. The appearance of small semicircle is probably ascribed to the interface resistance of active material/collector and the resistance between active material particles [26]. The almost vertical line suggests blocking electrode behavior. This very steep spike shows the fast diffusion of ions in the solution and the quick adsorption of ions onto the electrode surface. However, the equivalent series resistance (ESR, the intercept at the Z′-axis) of graphene/AC composite electrode (0.49 Ω) is lower than that of commercial AC electrode (0.89 Ω). This result indicates that graphene introduced into AC can significantly improve its conductivity.

In order to further test the performance of supercapacitor based on graphene/AC nanosheet composite and widen its application scopes, we constructed and measured the electrochemical properties of coin-cell symmetrical supercapacitor with commercial 1 M Et_4NBF_4/PC as the electrolyte. The CV testing (Fig. 8a) shows rectangular curves from 0 to 2.5 V over a wide range of scan rates (1–200 mV s^{-1}). It's observed that the CV shapes are not seriously distorted even at high scan rates, indicating the porous nanosheet composite is not only suitable for aqueous electrolytes, but also appropriate for organic electrolytes. The potential window broadens significantly in the organic electrolyte, which will further promote the energy density of graphene/AC nanosheet composite. The energy density was calculated according to Equation (1), and the power density was calculated by dividing the energy density by the discharge time (Equation (2)). The equations are listed below:

$$E = \frac{1}{2}CU^2 \tag{1}$$

$$P = \frac{E}{t_{\text{discharge}}} \tag{2}$$

where E is the energy density (Wh kg^{-1}), U is the potential (V), and P is the power density (W kg^{-1}). The Ragone plot of graphene/AC composite is shown in Fig. 8b. The energy density can reach 22.3 Wh kg^{-1} at a power density of 33.2 W kg^{-1}. The corresponding volumetric energy density and power density are calculated to be 15.9 Wh L^{-1} and 23.6 W L^{-1} (estimated based on the volume of active material layer on the current collector pressed under a pressure of 6 MPa), respectively. However, the energy density decreases with increasing power density, mainly because the mesopore content of the graphene/AC nanosheet composite is not enough. In contrast, the maximum energy density of commercial AC is 12.5 Wh kg^{-1} (11.1 Wh L^{-1}), which is lower than that of graphene/AC composite. Furthermore, the commercial AC electrode exhibits lower power densities, which mainly ascribes to the large dense particle structure of commercial AC and its poor conductivity.

The cyclic stability of supercapacitor is a crucial parameter for its practical applications. The long-term cyclic stability of the graphene/AC nanosheet composite was evaluated by repeating the CV test between 0 and 2.5 V at a scan rate of 100 mV s^{-1} for 5000 cycles. The relationship between capacitance retention ratio and cycle number is shown in Fig. 8c. The capacitance only decreases by 5.3% of the initial capacitance after 5000 cycles, and the shapes of CV curve before and after 5000 cycles are almost the same (Fig. 8c, inserted image), demonstrating excellent electrochemical stability of the flaky porous composite electrode.

In addition, the packing density of graphene/AC is near to that of commercial AC, which is far more than that of graphene. Active materials with higher volumetric density in supercapacitor electrode favor the increase of high volumetric energy density. Also due to the adjacent appearance density of the graphene/AC composite comparing with AC, this material can be easily manufactured using the current procedures for commercial AC-based supercapacitor. Furthermore, the unique "graphene embedded in AC" structure can endure long-term charge/discharge cycles. In comparison, the composite of carbon materials with metal oxide or conductive polymer usually suffer from quick fade of the capacity during long cycles. Finally, the hydrothermal carbonization method, in this work, can be easily scaled up and allows the use of any kinds of soluble carbon precursors, including biomass-based raw materials, which is important to prepare high-performance supercapacitor electrode materials with low cost.

4. Conclusions

In this paper, porous graphene/AC nanosheet composite has been fabricated by hydrothermal carbonization and subsequent two-step chemical activation with KOH. The specific capacitance based on composite material is 210 F g^{-1} in aqueous electrolyte and 103 F g^{-1} in organic electrolyte, respectively. The composite exhibits a low ESR and high ion diffusivity, and the electrode also shows excellent cyclic stability. The specific capacitance decreases by only 5.3% after 5000 cycles. The excellent electrochemical performance is mainly attributed to the unique nanosheet composite structure. In this composite material, a layer of porous AC derived from glucose coats on graphene, serving as spacer between graphene layers, which can improve the dispersion of graphene sheets and increase its packing density. The graphene integrated into AC matrix also increase the conductivity of AC. On the other hand, unlike large AC particles, the nanosheet-like electrode material has a short diffusion pathway, which facilitates the rapid transport of the electrolyte ions. Therefore, the graphene/AC nanosheet composite prepared by hydrothermal carbonization is a promising electrode material for supercapacitor with high performance.

Acknowledgments

This work was supported by National Nature Science Foundation of China (Grant No. 21201173), the Key Research program of the Chinese Academy of Sciences (Grant No. KGZD-EW-202-4), Ningbo Science and Technology Innovation Team (Grant No. 2012B82001), the 973 program (Grant No. 2011CB935900), the China Postdoctoral Science Foundation funded project (Grant No. 2013M531489) and the Programs Supported by Ningbo Natural Science (Grant No. 2013A61002).

References

[1] M. Mastragostino, F. Soavi, J. Power Sources 174 (2007) 89–93.
[2] Y.J. Kim, C.M. Yang, K.C. Park, K. Kaneko, Y.A. Kim, M. Noguchi, T. Fujino, S. Oyama, M. Endo, ChemSusChem 5 (2012) 535–541.
[3] K. Naoi, S. Ishimoto, J. Miyamoto, W. Naoi, Energy Environ. Sci. 5 (2012) 9363–9373.
[4] F. Zhang, T.F. Zhang, X. Yang, L. Zhang, K. Leng, Y. Huang, Y.S. Chen, Energy Environ. Sci. 6 (2013) 1623–1632.
[5] C. Zheng, W.Z. Qian, C.J. Cui, Q. Zhang, Y.G. Jin, M.Q. Zhao, P.H. Tan, F. Wei, Carbon 50 (2012) 5167–5175.
[6] A. Izadi-Najafabadi, S. Yasuda, K. Kobashi, T. Yamada, D.N. Futaba, H. Hatori, M. Yumura, S. Lijima, K. Hata, Adv. Mater. 22 (2010) E235–E241.
[7] Y.W. Zhu, S. Murali, M.D. Stoller, K.J. Ganesh, W.W. Cai, P.J. Ferreira, A. Pirkle, R.M. Wallace, K.A. Cychosz, M. Thommes, D. Su, E.A. Stach, R.S. Ruoff, Science 332 (2011) 1537–1541.
[8] C.G. Liu, Z.N. Yu, D. Neff, A. Zhamu, B.Z. Jang, Nano Lett. 10 (2010) 4863–4868.
[9] N. Jia, P. Ramesh, E. Bekyarova, M.E. Itkis, R.C. Haddon, Adv. Energy Mater. 2 (2012) 438–444.
[10] M.Q. Zhao, Q. Zhang, J.Q. Huang, G.L. Tian, T.C. Chen, W.Z. Qian, F. Wei, Carbon 54 (2013) 403–411.
[11] G.H. Yu, L.B. Hu, M. Vosgueritchian, H.L. Wang, X. Xie, J.R. McDonough, X. Cui, Y. Cui, Z.N. Bao, Nano Lett. 11 (2011) 2905–2911.
[12] J. Yan, Z.J. Fan, T. Wei, W.Z. Qian, M.L. Zhang, F. Wei, Carbon 48 (2010) 3825–3833.
[13] S. Biswas, L.T. Drzal, Chem. Mater. 22 (2010) 5667–5671.
[14] J.J. Xu, K. Wang, S.Z. Zu, B.H. Han, Z.X. Wei, ACS Nano 4 (2010) 5019–5026.
[15] A.V. Murgan, T. Muraliganth, A. Manthiram, Chem. Mater. 21 (2009) 5004–5006.
[16] K.S. Novoselov, A.K. Geim, S.V. Morozov, D. Jiang, Y. Zhang, S.V. Dubonos, I.V. Grigorieva, A.A. Firsov, Science 306 (2004) 666–669.
[17] J.L. Xia, F. Chen, J.H. Li, N.J. Tao, Nat. Nanotechnol. 4 (2009) 505–509.
[18] Y. Huang, J.J. Liang, Y.S. Chen, Small 8 (2012) 1805–1834.
[19] G.Q. Ning, Z.J. Fan, G. wang, J.S. Gao, W.Z. Qian, F. Wei, Chem. Commun. 47 (2011) 5976–5978.
[20] L.L. Zhang, X. Zhao, M.D. Stoller, Y.W. Zhu, H.X. Ji, S. Murali, Y.P. Wu, S. Perales, B. Clevenger, R.S. Ruoff, Nano Lett. 4 (2012) 1806–1812.
[21] Z.J. Fan, J. Yan, L.J. Lin, Q. Zhang, T. Wei, J. Feng, M.L. Zhang, W.Z. Qian, F. Wei, Adv. Mater. 33 (2010) 3723–3728.
[22] C. Zheng, W.Z. Qian, F. Wei, Mater. Sci. Eng. B 177 (2012) 1138–1143.
[23] C. Compton, S.T. Nguyen, Small 6 (2010) 711–723.
[24] Z.B. Lei, L. Lu, X.S. Zhao, Energy Environ. Sci. 5 (2012) 6391–6399.
[25] L. Zhao, L.Z. Fan, M.Q. Zhou, H. Guan, S.Y. Qiao, M. Antonietti, M.M. Titirici, Adv. Mater. 22 (2010) 5202–5206.
[26] C. Portet, P.L. Taberna, P. Simon, C. Laberty-Robert, Electrochim. Acta 49 (2004) 905–912.